PAPER

Nonlinear harmonics coupled by parallel wave propagations in a time-dependent plasma flow

To cite this article: Min Uk Lee *et al* 2022 *Plasma Phys. Control. Fusion* **64** 055005

View the article online for updates and enhancements.

Nonlinear harmonics coupled by parallel wave propagations in a time-dependent plasma flow

Min Uk Lee[1,2] , **Gunsu S Yun**[1,3,*] and **Jeong-Young Ji**[2,*]

[1] Department of Physics, Pohang University of Science and Technology, Pohang, Gyeongbuk 37673, Republic of Korea
[2] Department of Physics, Utah State University, Logan, UT 84322, United States of America
[3] Division of Advanced Nuclear Engineering, Pohang University of Science and Technology, Pohang, Gyeongbuk 37673, Republic of Korea

E-mail: gunsu@postech.ac.kr and j.ji@usu.edu

CrossMark

Abstract

In a time-dependent flow, nonlinear harmonics can be excited by coupling between linear waves and flow-induced harmonic waves. Examining the dispersion relations and selection rules for the coupling, we investigate nonlinearly coupled harmonics for waves propagating along the magnetic field line in a magnetized plasma, as well as waves in an unmagnetized plasma. The coupled harmonics in a plasma flow are described by analytic dispersion relations and selection rules. This nonlinear coupling is corroborated by the particle-in-cell simulation. The coupled-harmonics model describes a mechanism for the excitation of nonlinear harmonics from linear waves in a time-dependent flow. The spectral analysis of the dispersion relation provides a useful way to evaluate the spatiotemporal behavior of a plasma flow.

Keywords: plasma flow, fluid wave harmonics, wave-wave coupling

(Some figures may appear in colour only in the online journal)

1. Introduction

The temporal behavior of plasma flows and associated wave instabilities have been investigated in order to understand plasma dynamics. For magnetically confined plasmas, magnetohydrodynamic instabilities [1–3] have been studied in order to achieve stable confinement [4, 5]. On the other hand, instabilities in space plasmas, such as the ionosphere [6], magnetosphere [7], solar wind [8], coronal loop [9], and astrophysical jet [10, 11] have been studied in order to understand field and particle behavior.

Linear plasma theory provides a simple but useful way to analyze wave properties such as a dielectric tensor and a wave dispersion relation. One of the simplest models is the cold plasma wave [12]. The *cold* wave dispersion relation is derived from fluid equations for density and flow velocity. The relation is a good approximation for $\omega/k \gg v_T$, where ω is the angular frequency, k is the wavenumber, and v_T is the thermal speed. By considering higher-order moments of an arbitrary distribution function, the *warm* (fluid) wave dispersion relation, depending on temperature and non-Maxwellian moments, can be obtained [13, 14]. The Vlasov equation can be directly used to derive the *hot* (kinetic) wave dispersion relation [15]. The analysis of the hot plasma waves provides kinetic effects such as energy exchange between waves and resonant particles [16].

In the linear assumption, the modes are independent and their interaction is ignored. However, plasmas involve nonlinearly coupled fields and associated particle motions [17–20]. Even when the intensity of a nonlinearly excited wave is small compared to a linear wave, the nonlinear

---

wave can carry information of a plasma or trigger instabilities [17, 21–23]. By investigating the nonlinearity, one can understand plasma kinetics which cannot be explained by linear theory.

In our previous work [23], we reported a dispersion relation that involved the nonlinear coupling of a cold (or warm) wave and a hot wave via time-dependent plasma flows. As an example, the couplings between extraordinary waves (X-waves) are demonstrated by the Vlasov analysis and particle-in-cell (PIC) simulations, where the waves are electromagnetic and perpendicular to the equilibrium magnetic field. In this work, we examine the dispersion relation to study the nonlinear couplings between electrostatic and electromagnetic waves propagating along the magnetic field in a plasma. This analysis is also valid for waves in an unmagnetized plasma. The analytic relations derived from the Vlasov equation describe the excitation of harmonics due to the time-dependent flow. The fully kinetic PIC simulations demonstrate the nonlinear couplings of linear waves and the flow-induced harmonics. This spectral analysis of coupled harmonics is expected to provide a way of understanding plasma flows.

Nonlinear wave analysis followed by a generalized dielectric tensor is presented in section 2. The numerical verification by PIC simulations is shown in section 3. We summarize the results and discuss a possible application of the harmonic analysis in section 4.

2. Dispersion relation for coupled waves

We consider a time-varying plasma with a distribution function $f_s(t) = f_{s0}(t) + f_{s1}(t)$ that consists of the zeroth-order Maxwellian distribution:

$$f_{s0}(\mathbf{v},t) = \frac{n_{s0} \exp\left[-\frac{(\mathbf{v}_\perp - \mathbf{u}_{s0\perp})^2}{v_{Ts\perp}^2} - \frac{(\mathbf{v}_\parallel - \mathbf{u}_{s0\parallel})^2}{v_{Ts\parallel}^2}\right]}{\pi^{3/2} v_{Ts\perp}^2 v_{Ts\parallel}}, \quad (1)$$

and the first-order deviation f_{s1} ($\ll f_{s0}$), where s denotes the species, $n_{s0} = \bar{n}_{s0} + \tilde{n}_{s0}(t)$ ($\bar{n}_{s0} \gg \tilde{n}_{s0}$) is the number density, $\mathbf{u}_{s0} = \bar{\mathbf{u}}_{s0} + \tilde{\mathbf{u}}_{s0}(t)$ is the flow velocity, $v_{Ts} = (2T_{s0}/m_s)^{1/2}$ is the thermal speed, T_s is the temperature, m_s is the mass, and the subscripts $\perp$ and $\parallel$ mean perpendicular and parallel with respect to the equilibrium magnetic field $\bar{B}_0 \hat{z}$. The zeroth-order fields are decomposed into the time-independent part (denoted by a bar) and the time-dependent part (denoted by a tilde). The time-dependent plasma flow can be expressed as:

$$\tilde{\mathbf{u}}_{s0}(t) = \sum_{l=1}^{N} \sum_{r=1}^{3} \tilde{u}_{s0lr}(t) \hat{e}_r, \quad (2)$$

where $\tilde{u}_{s0lr}(t) = \tilde{u}'_{s0lr} \mathrm{Re}[\exp \mathrm{i}\phi_{slr}(t)]$ is the $\hat{e}_r$ component of the lth mode with the amplitude $\tilde{u}'_{s0lr}$, the fluid wave frequency $\tilde{\omega}_l = \tilde{\omega}_l(\tilde{\mathbf{k}}_l)$, and the phase shift ψ_{slr}, and $\phi_{slr}(t) = \tilde{\omega}_l t + \psi_{slr}$. The summation is over all fluid modes with $\tilde{\omega}_l$ for $1 \leqslant l \leqslant N$ and all vector components $\{e_1, e_2, e_3\} = \{x, y, z\}$, where N is the number of fluid modes considered to be presumed in the zeroth-order distribution function in equation

(1). The time-dependent flow $\tilde{\mathbf{u}}_{s0}$ and the associated fields $\tilde{\mathbf{E}}_0, \tilde{\mathbf{B}}_0$ can be normal modes or driven by external forces such as an RF source. As a normal mode, the frequency $\tilde{\omega}_l(\tilde{\mathbf{k}}_l)$ of the perturbations $(\tilde{\mathbf{u}}_{s0}, \tilde{\mathbf{E}}_0, \tilde{\mathbf{B}}_0)$ is determined by the dispersion relation obtained from the Vlasov equation for f_{s0} (or equivalently fluid equations) by assuming a small wavenumber ($|\tilde{\mathbf{k}}_l \cdot \tilde{\mathbf{u}}_{s0l}| \ll |\tilde{\omega}_l|$). The lowest order solution of the zeroth-order Vlasov equation ($\tilde{\omega}_l/\tilde{k}_l \gg v_{Ts}$) gives the cold wave dispersion relation and the associated mobility for $\tilde{\mathbf{u}}_{s0}$. By solving the linearized Vlasov equation for f_{s1}, $\mathbf{E}_1$, and $\mathbf{B}_1$, the dielectric tensor of the time-varying plasma is obtained [23].

From the generalized dielectric tensor of a time-varying plasma (equation (24) in reference [23]), we obtain a dielectric tensor for the parallel propagation ($k \rightarrow k_\parallel$),

$$\mathsf{K} = \mathsf{I} + \sum_s \frac{\omega_{ps}^2}{\omega k v_{Ts\parallel}} \sum_{\{m\}=-\infty}^{\infty} \left(\prod_{l=1}^{N} J_{m_l} e^{\mathrm{i}\Phi_l}\right) \boldsymbol{\kappa}, \quad (3)$$

with the component of $\boldsymbol{\kappa}$,

$$\kappa_{ab} = \left(\hat{a} \cdot \hat{b} + \mathrm{i}\hat{a} \times \hat{b} \cdot \hat{z}\right) \frac{1}{2} \times \left[\frac{\omega_{Ds} - \sum_{l=1}^{N} m_l \tilde{\omega}_l}{\omega}\right.$$
$$\times \left(Z(\zeta_{s\{m\},1}) + (2\delta_{ab} - 1) Z(\zeta_{s\{m\},-1})\right) + \frac{k v_{Ts\parallel}}{2\omega}$$
$$\left. \times \left(1 - \frac{T_{s0\perp}}{T_{s0\parallel}}\right) \left(Z'(\zeta_{s\{m\},1}) + (2\delta_{ab} - 1) Z'(\zeta_{s\{m\},-1})\right)\right]$$
$$\kappa_{zz} = -\left(\zeta_{s\{m\},0} + \frac{u_{s0\parallel}}{v_{Ts\parallel}}\right) Z'(\zeta_{s\{m\},0}), \quad (4)$$

where $\omega_{ps} = (q_s^2 n_{s0}/\varepsilon_0 m_s)^{1/2}$ is the plasma frequency, q_s is the charge, ε_0 is the vacuum permittivity, $\sum_{\{m\}=-\infty}^{\infty} = \sum_{m_1=-\infty}^{\infty} \cdots \sum_{m_N=-\infty}^{\infty}$ indicates the sum of respective ω_l mode contributions, m_l for $1 \leqslant l \leqslant N$ is integer, $J_{m_l} = J_{m_l}(k\tilde{u}'_{s0l\parallel}/\tilde{\omega}_l)$ is the Bessel function of the first kind, and $\Phi_l = m_l \phi_{sl\parallel} - (k\tilde{u}'_{s0l\parallel}/\tilde{\omega}_l) \sin \phi_{sl\parallel}$. In equation (4), the subscripts a and b denote x or y ($K_{xx} = K_{yy}$, $K_{xy} = -K_{yx}$, and $K_{zx} = K_{xz} = K_{zy} = K_{yz} = 0$). The plasma dispersion function $Z(\zeta)$ and its derivative $Z'(\zeta) = \mathrm{d}Z/\mathrm{d}\zeta$ are defined by:

$$Z(\zeta) = \frac{1}{\sqrt{\pi}} \int_{-\infty}^{\infty} \frac{e^{-\xi^2}}{\xi - \zeta} \mathrm{d}\xi, \quad (5)$$

and

$$\zeta_{s\{m\}n} = \frac{\omega_{Ds} - \sum_{l=1}^{N} m_l \tilde{\omega}_l - n\omega_{cs}}{k v_{Ts\parallel}}, \quad (6)$$

where $\omega_{Ds} = \omega - k\bar{u}_{s0\parallel}$ is the Doppler-shifted frequency, $\omega_{cs} = q_s \bar{B}_0/m_s$ is the cyclotron frequency, and the integer values of $\{m\} = \{m_1, \ldots, m_N\}$ in equations (4)–(6) are given by the summation $\sum_{\{m\}=-\infty}^{\infty}$ in equation (3). Note that because of the time-dependent flow effect $\tilde{\omega}_l$, the real part of the numerator of $\zeta_{s\{m\},0}$ can be zero near the fluid wave harmonics $\omega = \sum_{l=1}^{N} m_l \tilde{\omega}_l$. For example, when $N = 3$, the possible harmonics are $\omega = m_1 \tilde{\omega}_1 + m_2 \tilde{\omega}_2 + m_3 \tilde{\omega}_3$ for arbitrary integers m_1, m_2, and m_3.

With the dielectric tensor of equation (3) substituted into the wave equation $(\mathbf{nn} - n^2 \mathsf{I} + \mathsf{K}) \cdot \mathbf{E}_1 = 0$ (combination of Faraday's and Ampère's laws), the vanishing determinant yields the dispersion relations, for electromagnetic waves ($\mathbf{E}_1 = E_{1x}\hat{x} + E_{1y}\hat{y}$),

$$\mathcal{D}_R(\omega, k) = K_{xx} - n^2 + \mathrm{i}K_{xy} = 0, \qquad (7)$$

$$\mathcal{D}_L(\omega, k) = K_{xx} - n^2 - \mathrm{i}K_{xy} = 0, \qquad (8)$$

and, for the electrostatic waves ($\mathbf{E}_1 = E_{1\parallel}\hat{z}$),

$$\mathcal{D}_{\mathrm{ES}}(\omega, k) = K_{zz} = 0, \qquad (9)$$

where $\mathbf{n} = c\mathbf{k}/\omega$ is the refractive index and c is the speed of light. Equations (7) and (8), respectively, are the dispersion relations for the right-hand circularly polarized wave (R-wave) and left-hand circularly polarized wave (L-wave).

Note that the dispersion relations for waves in an unmagnetized plasma should be reproduced from the above dispersion relations by setting $\bar{B}_0 = 0$. For electromagnetic waves, equations (7) and (8) become:

$$\mathcal{D}_{\mathrm{EM}}(\omega, k) = K_{xx} - n^2 = 0, \qquad (10)$$

where $Z(\zeta_{s\{m\},\pm 1}) = Z(\zeta_{s\{m\},0})$, $T_{s0\perp}/T_{s0\parallel} - 1 = 0$, and $\kappa_{xx} = (\omega_{Ds} - \sum_{l=1}^{N} m_l\tilde{\omega}_l)Z(\zeta_{s\{m\},0})/\omega$ in equation (4). For electrostatic waves, the dispersion relation is clearly the same as equation (9). When the zeroth-order flow is ignored by $\bar{u}_{s0} = 0$ ($\omega_{Ds} \to \omega$) and $\tilde{u}'_{s0} = 0$, the dielectric tensor and the dispersion relations in equations (3)–(10) reduce to those of the conventional hot waves [15]. This is because in equation (3), only $m_l = 0$ terms remain ($J_{m_l \neq 0}(0) = 0$, $J_{m_l=0}(0) = 1$, $\Phi_l = 0$, and $\zeta_{s\{m\}n} \to \zeta_{sn}$).

Equation (6) shows that the dispersion relation $\mathcal{D}(\omega, k) = 0$ in the time-dependent flow can generate the fluid wave harmonics $\omega \simeq \sum_{l=1}^{N} m_l\tilde{\omega}_l$. Figure 1 shows fluid wave harmonics for a deuterium plasma of $n_{e0} = n_{i0} = 10^{19}$ m^{-3} and $T_{e0} = T_{i0} = 1$ keV in $B_0 = 2$ T. For a single mode of $\tilde{\omega}$, the harmonics $\omega \simeq m\tilde{\omega}$ appear in the dispersion relation in addition to the conventional hot-wave mode $\bar{\omega}$, where $\bar{\omega}$ denotes the frequency satisfying $\mathcal{D} = 0$ for the time-independent plasma (green dashed line). The fluid wave harmonics have finite damping rates $|\mathrm{Im}(\omega)|$ and the damping rate increases as the harmonic number increases.

Nonlinear harmonic waves have been observed with plasma flows, such as in magnetotail reconnection [25, 26] and solar radio bursts [27–30]. The emission mechanism has been well explained by the quasi-linear and weak-turbulence theories [28]. The nonlinear theories describe the interactions between an electron beam and three types of waves in a weakly magnetized plasma (Langmuir, ion-sound, and electromagnetic waves). Since general flows and wave dispersion relations are analyzed in this work, one is able to describe the nonlinear harmonic interactions induced by general fluid waves and hot waves such as O/X-waves, R/L-waves, and electrostatic
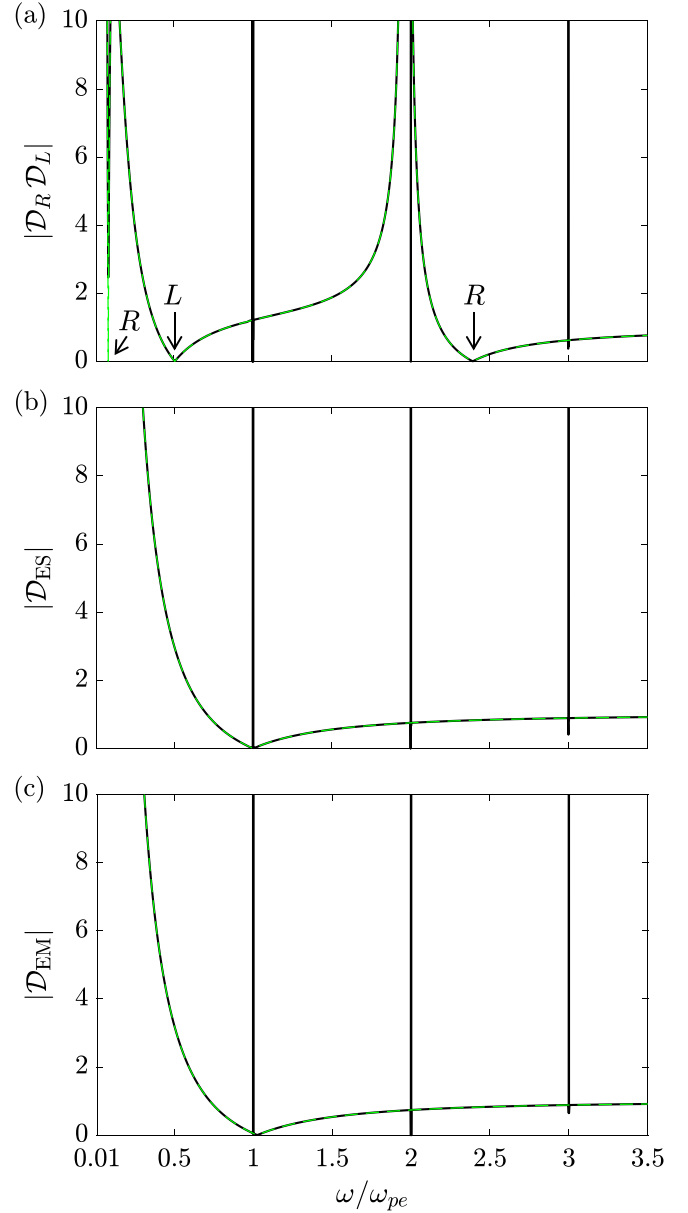

Figure 1. Analytic calculations of $\mathcal{D}$ for (a) the electromagnetic wave in the magnetized plasma (equations (7) and (8)), (b) the electrostatic wave (equation (9)), and (c) the electromagnetic wave in the unmagnetized plasma (equation (10)). The values of $\mathcal{D}$ are plotted for the time-independent plasma (green dashed line, $\mathrm{Im}(\omega) = 0$) and the time-dependent plasma (solid line, $\tilde{\omega} = \omega_{pe}$, $\tilde{u}_{e0\parallel} = 10^{-2}v_{Te}$, and $\mathrm{Im}(\omega) = -2 \times 10^{-3}\omega_{pe}$), where $\lambda_{De} = (\varepsilon_0 T_{e0}/n_{e0}q_e^2)^{1/2}$ is the electron Debye length (for simplicity, the ω axis in the figures denotes the real part of the frequency). They show the fluid wave harmonics $\omega \simeq m\tilde{\omega}$. The plasma dispersion function is obtained by using the algorithm described in [24].

waves. Fully kinetic PIC simulations showed that a nonlinear coupling between the conventional mode $\bar{\omega}$ and the fluid wave harmonics $\sum_{l=1}^{N} m_l\tilde{\omega}_l$ satisfies the wavenumber selection rule [23]:

$$\omega \simeq \bar{\omega} + \sum_{l=1}^{N} m_l\tilde{\omega}_l. \qquad (11)$$
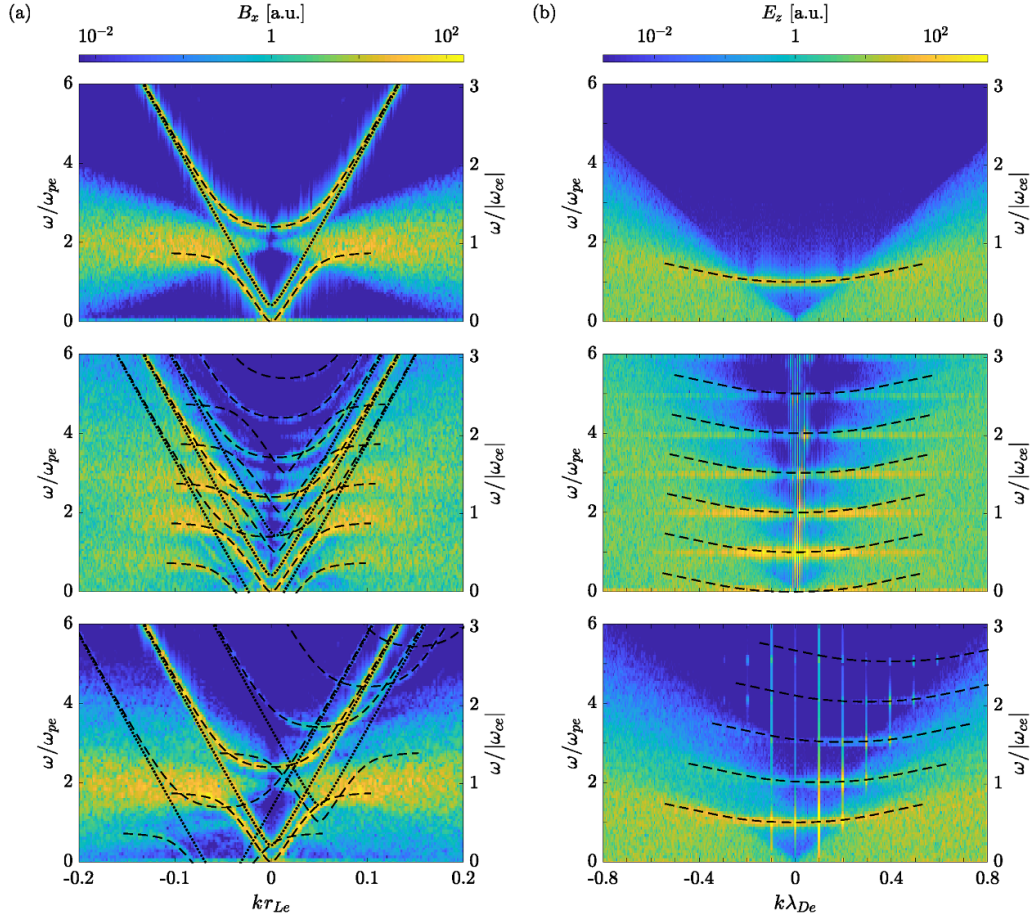
Figure 2. Field intensities from PIC simulations for the magnetized plasma: (a) B_x for the electromagnetic mode, (b) E_z for the electrostatic mode. The panels show the results when $\tilde{\mathbf{u}}_0 = 0$ (top) and $\tilde{\mathbf{u}}_0 = \tilde{\mathbf{u}}_{0\parallel}(\tilde{\omega} \simeq \omega_{pe}, \tilde{k})$ for $\tilde{k}\lambda_{De} = 10^{-2}$ (middle) and $\tilde{k}\lambda_{De} = 10^{-1}$ (bottom); $\lambda_{De} = 2r_{Le}$. Analytic dispersion relations are overlaid for (a) the *R*-wave (dashed lines) and *L*-wave (dotted lines) for a damping rate $|\text{Im}(\bar{\omega})| < 0.1|\omega_{ce}|$, and overlaid for (b) the electron plasma wave (dashed line) for $|\text{Im}(\bar{\omega})| < 0.1\omega_{pe}$. The coupled harmonics overlaid in the middle and bottom panels are plotted from $\bar{\omega}(\bar{k})$ and the selection rules for several *m*. It is observed that a strongly damped *R*-mode, an electron plasma mode, and higher harmonics have weaker intensities as predicted by the analytic dispersions.
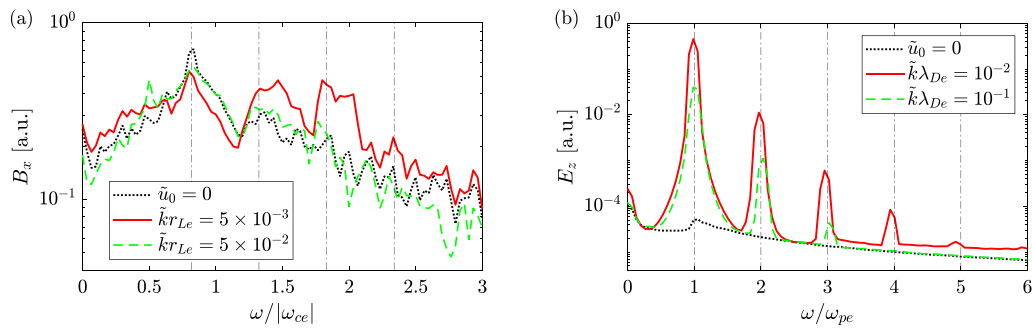

Figure 3. Temporal Fourier transforms of field intensities for figures 2(a) and (b). The dash-dotted lines indicate the coupled harmonics $\omega = \bar{\omega} + m\tilde{\omega}$.

For example, the conventional cyclotron harmonics $\bar{\omega} \simeq n\omega_{cs}$ due to thermal motions and the fluid wave harmonics $\sum_{l=1}^{N} m_l\tilde{\omega}_l$ due to plasma flows excite the harmonics $\omega \simeq n\omega_{cs} + \sum_{l=1}^{N} m_l\tilde{\omega}_l$. On the other hand, from various studies of the coupling between oscillation modes [31–35], it has been shown that the coupling may satisfy the wavenumber selection rule as well as the frequency selection rule. The wavenumber selection rule associated with equation (11) is:

$$\mathbf{k} \simeq \bar{\mathbf{k}} + \sum_{l=1}^{N} m_l\tilde{\mathbf{k}}_l. \tag{12}$$

The combination of the linear dispersion relation (equations (3)–(10)) and the selection rules (equations (11) and (12)) provides the dispersion relation for the nonlinearly coupled harmonics in a time-dependent plasma. The selection rules and

4

the associated nonlinear dispersions are verified using the PIC simulation [33, 35].

In equation (3), we reveal that the time-dependent flow ($m_l \neq 0$ terms) contributes to the wave dispersion relation only when the longitudinal flow amplitude $\tilde{u}'_{s0l\parallel}$ is finite since $J_{m_l \neq 0}(0) = 0$. This means that the longitudinal flow motion is the origin of the fluid wave harmonics $\sum_{l=1}^{N} m_l \tilde{\omega}_l$ and the resulting wave-wave coupling. For a perpendicular propagating wave in a magnetized plasma, the electromagnetic *X*-wave produces a longitudinal flow resulting in the coupling between electromagnetic waves [23]. For a parallel propagating wave, the electrostatic wave drives the coupled harmonics since the longitudinal flow oscillation ($\tilde{\omega} \simeq \omega_{pe}$ in a small wavenumber limit) is only associated with the electrostatic wave.

It is shown analytically that the wave nonlinearity provides the excitation mechanism of the coupled harmonics (equations (11) and (12)) induced by a plasma flow of $\tilde{\omega}(\tilde{\mathbf{k}})$. In section 3, the dispersion relations for the nonlinear couplings between the electrostatic waves and other waves are demonstrated by the PIC simulation.

3. Particle-in-cell simulation

We demonstrate the coupled harmonics by using PIC simulations [36] in the one-dimensional position (periodic boundary condition in the *z* direction) and three-dimensional velocity space. The reliability and convergence of the numerical simulation have been confirmed as follows. The spatial grid is less than 3% of the electron Debye length λ_{De} while the total length is longer than $10^3 \lambda_{De}$, including several wavelengths of the initial perturbation. The time step satisfies the Courant–Friedrichs–Lewy criterion for the given spatial grid. The number of superparticles per cell is of the order of 10^4 (corresponding to the order of 10^5 per λ_{De}). The energy conservation has been confirmed and an instability has not been observed.

Considering the plasma condition used in figure 1, we examine the dispersion relation satisfying the selection rules for coupled harmonics excited by a time-dependent flow of $\tilde{\omega}(\tilde{k})$. Initiating an electron plasma wave with density perturbation $\tilde{n}_{e0}(x)/\bar{n}_{s0} = 0.05 \cos(\tilde{k}x)$ with $\tilde{\omega} \simeq \omega_{pe}$, we observe the excitation of coupled harmonics in the simulation. The initial profiles of $\tilde{n}_0$, $\tilde{\mathbf{u}}_{0\parallel}$, and $\tilde{E}_{0\parallel}$ are determined by the zeroth-order Vlasov equation and Maxwell's equations. We compare the analytic dispersion relation and the spatiotemporal Fourier transform of the simulation result. From the dispersion relation for $\bar{\omega}(\bar{k})$ of the time-independent plasma, we can obtain the dispersion for the coupled harmonics by using the selection rules $\omega = \bar{\omega} + m\tilde{\omega}(\tilde{k})$ and $k = \bar{k} + m\tilde{k}$.

Figure 2 shows the simulation results when the electrostatic wave is initially perturbed in the magnetized plasma. The analytic solutions overlaid on the simulation results confirm the nonlinearly coupled harmonics. The frequency selection rule $\omega \simeq \bar{\omega} + m\tilde{\omega}$ and the wavenumber selection rule $k = \bar{k} + m\tilde{k}$ are also confirmed in the middle and bottom panels. The frequency spectrum in figure 3 clearly shows the coupled harmonics $\omega \simeq \bar{\omega} + m\tilde{\omega}$.
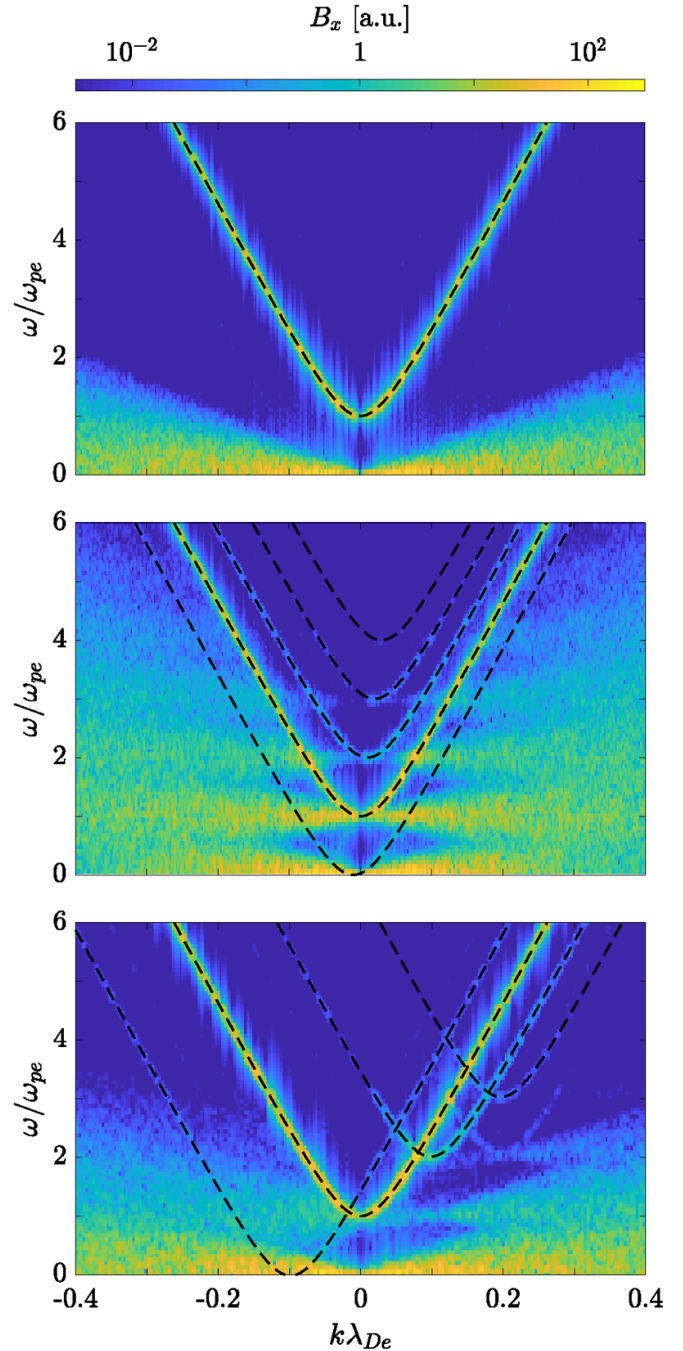

Figure 4. B_x intensities from PIC simulations for the unmagnetized plasma. The panels show the results when $\tilde{\mathbf{u}}_0 = 0$ (top) and $\tilde{\mathbf{u}}_0 = \tilde{\mathbf{u}}_{0\parallel}(\tilde{\omega} \simeq \omega_{pe}, \tilde{k})$ for $\tilde{k}\lambda_{De} = 10^{-2}$ (middle) and $\tilde{k}\lambda_{De} = 10^{-1}$ (bottom). Analytic dispersion relations are overlaid as described in figure 2.

Figure 4 shows the simulation results for the unmagnetized plasma, where the conditions are the same as in figure 2 except that $\bar{B}_0 = 0$. Comparison of the analytic and numerical results demonstrates the coupled electromagnetic harmonics. In the frequency spectrum, only the ω_{pe} harmonics were observed as seen in figure 4 middle. This is because, unlike for the waves in the magnetized plasma, the spectral peak does not exist in the electromagnetic spectrum of the unmagnetized

plasma wave. The simulation results for the electrostatic wave in the unmagnetized plasma are the same as figure 2(b), as expected.

In addition to the examples shown above, we have confirmed the selection rules for multiple $\tilde{\omega}_l(\tilde{k}_l)$. It has been observed that the intensities of the coupled harmonics increase as the amplitude of a time-dependent flow increases.

4. Summary and discussion

We study nonlinearly coupled harmonics by investigating the dispersion relation for parallel propagating waves in a time-dependent plasma flow. The analytic dispersion relations are derived from a generalized dielectric tensor of the time-dependent plasma. The dispersion relations show that harmonics of the fluid plasma wave are generated in addition to the conventional hot plasma wave. It is demonstrated that a coupling between a hot wave and fluid wave harmonics drives nonlinearly coupled harmonics, satisfying the frequency and wavenumber selection rules. The kinetic analysis reveals that the fluid wave harmonics and the resulting nonlinearity are induced by the flow motion longitudinal to the wave propagation. The coupled harmonics are corroborated by the fully kinetic particle-in-cell simulation. Fourier transforms of the simulation results reproduce the coupled harmonics, as predicted by the kinetic analysis. The coupled harmonics appearing in the time-dependent plasma illustrate a mechanism for the nonlinear wave excitation from linear waves.

The coupled-harmonics theory in this work provides a useful way to interpret plasma flow behavior. The kinetic analysis and PIC simulations demonstrate that the spectral analysis of a plasma wave can display the $\tilde{\omega}(\tilde{\mathbf{k}})$ of a plasma flow. For example, the spectral analysis can be used for plasma diagnostics to measure flow scales via harmonic frequency. This is because when a flow perturbation such as an instability is initiated in the plasma, the spatial wavenumber $\tilde{\mathbf{k}}$ of the flow can generate the corresponding fluid oscillation $\tilde{\omega}(\tilde{\mathbf{k}})$. This wave can excite the nonlinearly coupled harmonics, satisfying the frequency and wavenumber selection rules, which can be analyzed by the dispersion relations, as in this paper.

We have found that flow-induced wave coupling originates from the time-dependent fluid motion which is longitudinal to the wave propagation. This coupling mechanism can be examined in a more general situation where the wave propagations are not parallel to each other. For example, when an R-wave propagates along the magnetic field line, the associated fluid mode oscillates in the direction perpendicular to the magnetic field. Since the flow oscillation is longitudinal to an X-wave that propagates perpendicular to the magnetic field, coupling between the R-wave and the X-wave can occur. If one measures the coupled X-wave (e.g. harmonics of electron cyclotron emission), the embedded R-wave modulation can be detected. This situation is similar to the recent observation [37], where a whistler wave (quasi-parallel R-wave), along with fluid instabilities, was detected by measuring the wave that propagates perpendicular to the magnetic field. The

experimentally observed coupling can be investigated by two-dimensional PIC simulations.

ORCID iDs

Min Uk Lee ⓘ https://orcid.org/0000-0003-0528-3583
Gunsu S Yun ⓘ https://orcid.org/0000-0002-1880-5865
Jeong-Young Ji ⓘ https://orcid.org/0000-0002-8735-7859

References

[1] Hastie R J, Ramos J J and Porcelli F 2003 Drift ballooning instabilities in tokamak edge plasmas *Phys. Plasmas* **10** 4405
[2] Webster A J 2012 Magnetohydrodynamic tokamak plasma edge stability *Nucl. Fusion* **52** 114023
[3] Ida K, Kobayashi T, Yoshinuma M, Akiyama T, Tokuzawa T, Tsuchiya H, Itoh K and Itoh S-I 2018 Trigger mechanism for the abrupt loss of energetic ions in magnetically confined plasmas *Sci. Rep.* **8** 2804
[4] Morris A W 1992 MHD instability control, disruptions and error fields in tokamaks *Plasma Phys. Control. Fusion* **34** 1871–9
[5] Graves J P, Chapman I T, Coda S, Lennholm M, Albergante M and Jucker M 2008 Control of magnetohydrodynamic stability by phase space engineering of energetic ions in tokamak plasmas *Nat. Commun.* **3** 624
[6] Heelis R A 2004 Electrodynamics in the low and middle latitude ionosphere: a tutorial *J. Atmos. Sol.-Terr. Phys.* **66** 825–38
[7] Faganello M and Califano F 2017 Magnetized kelvin-helmholtz instability: theory and simulations in the earth's magnetosphere context *J. Plasma Phys.* **83** 535830601
[8] Stansby D, Horbury T S, Chen C H K and Matteini L 2016 Experimental determination of whistler wave dispersion relation in the solar wind *Astrophys. J.* **829** L16
[9] Antolin P 2019 Thermal instability and non-equilibrium in solar coronal loops: from coronal rain to long-period intensity pulsations *Plasma Phys. Control. Fusion* **62** 014016
[10] Birkinshaw M 1996 Instabilities in astrophysical jets *Astrophys. Space Sci.* **242** 17–91
[11] Bellan P M 2020 Analytic model for the time-dependent electromagnetic field of an astrophysical jet *Astrophys. J.* **888** 69
[12] Stix T H 1992 *Waves in Plasmas* (New York: American Institute of Physics)

[13] Ji J-Y and Held E D 2008 Landau collision operators and general moment equations for an electron-ion plasma *Phys. Plasmas* **15** 102101

[14] Liang Wang A H Bhattacharjee H, A and Germaschewski K 2015 Comparison of multi-fluid moment models with particle-in-cell simulations of collisionless magnetic reconnection *Phys. Plasmas* **22** 012108

[15] Swanson D G 2003 *Plasma Waves (Series in Plasma Physics)* 2nd edn (London: Taylor and Francis) p 15

[16] Besse N, Elskens Y, Escande D F and Bertrand P 2011 Validity of quasilinear theory: refutations and new numerical confirmation *Plasma Phys. Control. Fusion* **53** 025012

[17] Gould R W, O'Neil T M and Malmberg J H 1967 Plasma wave echo *Phys. Rev. Lett.* **19** 219–22

[18] Malmberg J H, Wharton C B, Gould R W and O'Neil T M 1968 Plasma wave echo experiment *Phys. Rev. Lett.* **20** 95–7

[19] Das G C, Sarma J, Gao Y-T and Uberoi C 2000 Dynamical behavior of the soliton formation and propagation in magnetized plasma *Phys. Plasmas* **7** 2374–80

[20] Abdelwahed H G, Abdelrahman M A E, Inc M and Sabry R 2020 New soliton applications in earth's magnetotail plasma at critical densities *Front. Phys.* **8** 181

[21] Lesur M *et al* 2016 Nonlinear excitation of subcritical fast ion-driven modes *Nucl. Fusion* **56** 056009

[22] Woods J Q B 2019 Analytical solutions for nonlinear plasma waves with time-varying complex frequency *Plasma Res. Express* **1** 045003

[23] Lee M U, Ji J-Y and Yun G S 2020 Cold-hot coupled waves in a flowing magnetized plasma *Nucl. Fusion* **60** 126036

[24] Zaghloul M R and Ali A N 2012 Algorithm 916: computing the faddeyeva and voigt functions *ACM Trans. Math. Softw.* **38** 15

[25] Burch J L *et al* 2019 High-frequency wave generation in magnetotail reconnection: linear dispersion analysis *Geophys. Res. Lett.* **46** 4089–97

[26] Dokgo K, Kyoung-Joo Hwang J L Burch E C, Yoon P H, Sibeck D G and Graham D B 2019 High-frequency wave generation in magnetotail reconnection: nonlinear harmonics of upper hybrid waves *Geophys. Res. Lett.* **46** 7873–82

[27] Rhee T, Ryu C-M, Minho Woo H H Kaang S Y and Yoon P H 2009 Multiple harmonic plasma emission *Astrophys. J.* **694** 618–25

[28] Ratcliffe H, Brady C S, Che Rozenan M B and Nakariakov V M 2014 A comparison of weak-turbulence and particle-in-cell simulations of weak electron-beam plasma interaction *Phys. Plasmas* **21** 122104

[29] Ziebell L F, Yoon P H, Petruzzellis L T, Gaelzer R and Pavan J 2015 Plasma emission by nonlinear electromagnetic processes *Astrophys. J.* **806** 237

[30] Lee S-Y, Ziebell L F, Yoon P H, Gaelzer R and Lee E S 2019 Particle-in-cell and weak turbulence simulations of plasma emission *Astrophys. J.* **871** 74

[31] Manley J M and Rowe H E 1956 Some general properties of nonlinear elements-part I. general energy relations *Proc. IRE* **44** 904–13

[32] Bellan P M 2008 *Fundamentals of Plasma Physics* (Cambridge: Cambridge University Press)

[33] Gan C, Xiang N, Jing O and Zhi Y 2015 Particle-in-cell simulations of parametric decay instability of radiofrequency wave in the ion cyclotron range of frequency in an inhomogeneous plasma *Nucl. Fusion* **55** 063002

[34] Hansen S K, Nielsen S K, Stober J, Rasmussen J, Salewski M and Stejner M 2019 Power threshold and saturation of parametric decay instabilities near the upper hybrid resonance in plasmas *Phys. Plasmas* **26** 062102

[35] Senstius M G, Nielsen S K, Vann R G and S K Hansen 2019 Particle-in-cell simulations of parametric decay instabilities at the upper hybrid layer of fusion plasmas to determine their primary threshold *Plasma Phys. Control. Fusion* **62** 025010

[36] Arber T D *et al* 2015 Contemporary particle-in-cell approach to laser-plasma modelling *Plasma Phys. Control. Fusion* **57** 113001

[37] Kim M H, Thatipamula S G, Kim J, Choi M J, Lee J, Lee W, Kim M, Yoon Y D and Yun G S 2020 Intense whistler-frequency emissions at the pedestal collapse in KSTAR H-mode plasmas *Nucl. Fusion* **60** 126021